This is a manuscript of an article that was accepted in June 2017 for publication in the Journal of the American Water Resources Association. The final publication is available at http://dx.doi.org/10.1111/1752-1688.12537.

METHOD FOR RAPIDLY ASSESSING THE OVERTOPPING RISK OF BRIDGES DUE TO FLOODING OVER A LARGE GEOGRAPHIC REGION

Yawen Shen, Jonathan L. Goodall, Steven B. Chase

Graduate Research Assistant (Shen), Associate Professor (Goodall), and Research Professor (Chase), Department of Civil and Environmental Engineering, University of Virginia, 351 McCormick Road, Charlottesville, VA 22904. (E-Mail/Goodall: goodall@virginia.edu)

ABSTRACT: Hydraulic events are a leading cause of bridge failures. While these hydraulic events are accounted for in bridge design, changing environmental and land use conditions require continual updating of this risk. Streamflow, for example, can change after a bridge has been constructed in unanticipated ways as a result of land use changes, geomorphic changes, and climate change. The objective of this research is to create a screening method able to quickly and inexpensively estimate overtopping risk across a collection of bridges based on current streamflow conditions. The method uses a geographic information system (GIS), nationally available and standardized datasets, and recent regression equations to quantify bridge vulnerability to overtopping for flooding with varying return periods. This screening method could also be used to assist decision makers in updating the Waterway Adequacy field in the National Bridge Inventory (NBI), which indicates the overtopping risk of bridges. The method was applied for a portion of the Hampton Roads region of Virginia, USA that includes 475 bridges. The results of the analysis, when combined with transportation data for bridges, aid decision makers to assign further resources to complete more detailed analyses of bridges identified as being at risk for overtopping.

(KEY TERMS: bridge; vulnerability; overtopping; flooding; transportation infrastructure.)

INTRODUCTION

Hydraulic events are a leading cause of bridge failures (ASSHTO, 2004; Lee et al., 2013; Wardhana and Hadipriono, 2003). Bridge failure from hydraulic events is caused by various factors including riverbed scour at bridge foundations, hydrodynamic forces at bridge superstructure, overtopping, and debris accumulations (Parola et al., 1998; Okeil and Cai, 2008; and Bala et al., 2005). Riverbed scour at bridge foundations is the main reason for bridge damage (Melville and Coleman 2000) and, therefore, has attracted significant attention. In prior studies, many methods have been developed to measure or predict scour depth, such as radar and sonar (Park et al., 2004; Hunt, 2005), numerical and laboratory models (Richardson and Panchang, 1998; Deng and Cai, 2010), empirical equations (Jain and Fischer, 1979; and Melville, 1992), and machine learning models (Lee et al., 2007; and Zounemat-Kermani et al. 2009). Another important cause of damage to bridges, especially on approach embankment, is overtopping. For example, a large flood with a return period in excess of 500 years occurred in Atlanta, Georgia in 2009 causing significant damage to bridge abutments and embanks due to overtopping (Hong and Strum, 2010). Overtopping also results in changes to the scour depth and patterns near the riverbed (Guo, 2011; Shan et al., 2012). Significant research has been devoted to hydrodynamic forces on a submerged bridge resulting from overtopping because the drag and lift forces of submerged flow are a serious threat to the stability of the bridge deck (Malavasi et al., 2001; Cigada et al., 2001; Kara et al., 2015).

Bridges are designed to accommodate a discharge with a given return period, but these designs are based on current conditions and estimates of future conditions when the bridge was built (VDOT, 2014). However, future conditions, including climate, land use, and stream patterns, may experience unanticipated changes (Loaiciga, 2001; Bonnin et al., 2011; Bouska

and Stoebner, 2015). These changes can impact overtopping risk to bridges by affecting the drainage basin response to storm events of different return periods. For example, the intensity and spatial distribution of storm events with certain return periods may change significantly as a result of climate change (Tucker, 1997; Yang et al., 2010; Khelifa et al., 2013). The watershed draining to the bridge may experience a higher rate of land development than was anticipated, causing changes in the runoff characteristics including both the peak flow rate and the timing of the peak flow for a given storm event (Li, 2007; Bouska and Stoebner, 2015). Also, stream patterns change over time because of sediment transport and geomorphological processes, which could accelerate with more frequent extreme flooding events and human activities (Loaiciga, 2001; Yang et al. 2002; Hu et al., 2011). Therefore, under the influence of these uncertain future conditions, the characteristics of overtopping events for a given bridge may change significantly over its design life. This uncertainty highlights the need for periodical reassessments of the overtopping risk for a collection of bridges.

The overtopping risk for a bridge is included the National Bridge Inventory (NBI) as the Waterway Adequacy field. The Waterway Adequacy field appraises the waterway opening with respect to passage of flow through the bridge (FHWA, 1995). The rating given to a bridge this field is tied to overtopping frequencies and traffic delays. The overtopping frequency signed to each bridge is based on the inspection of field conditions: (1) high water marks immediately after peak flow events; (2) potential drainage area changes due to upstream structure construction, replacement, or removal; (3) scour; (4) accumulation of debris and sediment (FHWA, 2012). The method proposed in this paper, can assist in populating the Waterway Adequacy field in the NBI by taking into account watershed and environmental characteristics based on the best known current conditions stored within geospatial datasets.

Assessing this risk of overtopping is difficult because it requires the analysis of a potentially large watershed upstream of the bridge structure. While hydraulic and hydrology models are commonly used for this analysis, they are time consuming to set up, calibrate, and validate. This model set up process would need to be repeated for each bridge individually, making the approach even more impractical when bridge owners need to evaluate hundreds or thousands of bridges. Alternative approaches are needed that can quickly assess the overtopping risk for a large number of bridges based on recent streamflow information. While such approaches would lack detail compared to using well-calibrated hydrologic and hydraulic models, they would provide useful information at a lower cost across a large geographic region. This information could then be used to target remaining resources to those bridges identified as being most at risk. The process would offer a screening approach, therefore, able to assess a large number of bridges in order to target limited resources to a smaller subset of the bridges.

The objective of this study is to design such a screening method able to evaluate the risk of overtopping for a collection of bridges over a large geographic region. The method makes use of a geographic information system (GIS), nationally available and standardized geospatial datasets, streamflow regression equations developed by federal (i.e., the United States Geological Survey) and local (e.g., State Departments of Transportation) agencies. The method can be used to analyze a large number of bridges at once. This allows bridge owners to gain an understanding of their vulnerability to overtopping on a more regular basis as updated geospatial data and peak flow regression equations become available.

The remainder of the paper is organized as follows. The methodology section provides details on the steps for implementing the bridge overtopping screening tool. An example application is then presented applying the screening tool for a portion of the Hampton Roads

region of Virginia. The paper concludes with a discussion of the benefits and limitations of the approach, along with possible future research to further advance the approach.

METHODOLOGY

Bridges are overtopped if the water surface elevation at peak flow is above the bridge deck elevation. Assuming that the bridge deck elevation is known, the key task is to determine the water surface elevation at each bridge location during peak flow conditions. This is accomplished using five main steps (Figure 1): (1) data gathering; (2) computing peak flow rates at selected return periods for all bridge locations; (3) estimating the river cross-section geometry for all bridge locations; (4) estimating peak water surface elevation at selected return periods for all bridge locations; and (5) comparing the peak water surface elevation with the bridge deck elevation for all bridge locations. Details for each step are included in the following subsections.

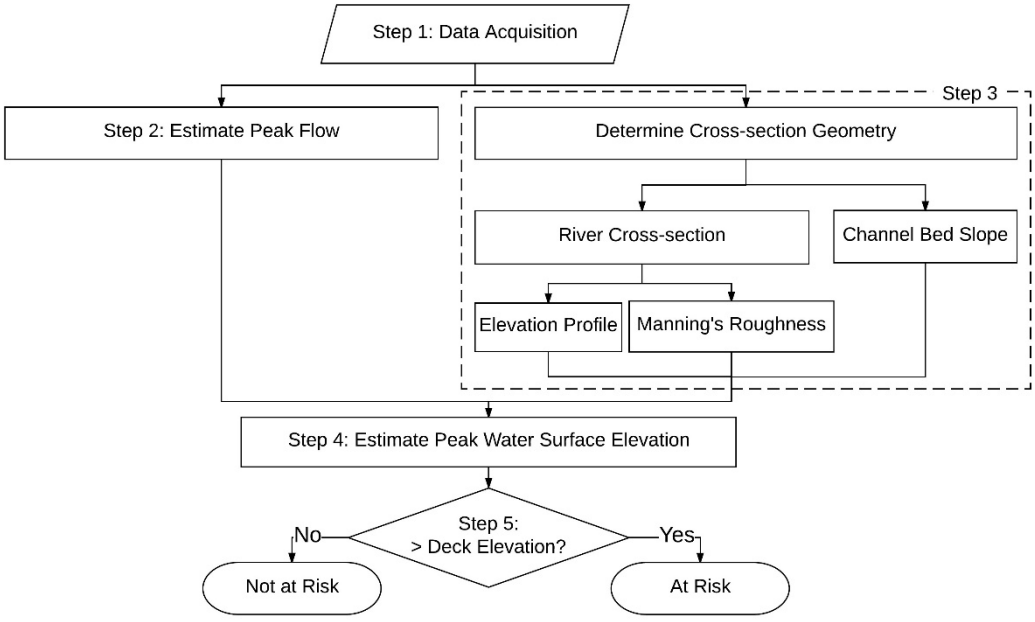

FIGURE 1. Procedure to Assess Vulnerability of Bridges to Overtopping Due to a Flooding Event with a Given Return Period

Data Gathering

The data used in this method are: (1) floodplain maps provided by the Federal Emergency Management Agency (FEMA); (2) watershed characteristics, such as catchment boundary, flowlines, flow accumulation, flow direction, and waterbody (e.g., products in National Hydrography Dataset (NHD)); (3) bridge properties including deck elevation and location (latitude and longitude); (4) a road network with the annual average daily traffic (AADT) for each road link; (5) a high resolution digital elevation model (DEM) dataset; and (6) a land cover dataset (e.g., the National Land Cover Dataset (NLCD)). The data are gathered for the study region from the various data providers and then organized for later progressing.

Estimate Peak Flow Rate at Bridge Locations for Different Storm Return Periods

The peak flow rate is estimated using regression-based tools and equations. The United States Geological Survey (USGS) has developed such equations for many regions in the United States. Many state Departments of Transportation (DOTs) have also developed regression equations for regions of their state (e.g., MnDOT, 2000; MDOT, 2006; VDOT, 2014; WSDOT, 2015). The subsections below provide examples of how to determine peak flow rates from the USGS using their StreamStats application (http://water.usgs.gov/osw/StreamStats/). The Virginia Department of Transportation Drainage Manual (VDOT 2014) is also presented as an example of regression equations developed by a state DOT.

USGS StreamStats Application. StreamStats is a Web application able to provide estimates of watershed characteristics and streamflow statistics at user-selected sites. The system has a user interface that allows for analysis at a single site or batch processing for multiple sites.

The tool provides a snapping feature that can be used to geolocate bridges to locations along the stream network. Once a location along the stream network has been determined, StreamStats is able to delineate the watershed for that location. This watershed is then used to derive watershed characteristics including estimates of the 5-year, 10-year, 25-year, 50-year, 100-year, and 200-year peak flow rates at the selected locations.

DOT Regression Equations. Regression equations developed for use by DOTs are commonly available for estimating peak flow rates at sites. These regression equations have been shown to be accurate, reliable, and provide consistent findings when utilized by different hydraulic engineers (Newton and Herrin, 1982). State DOTs commonly have a drainage manual that includes the regression equations for estimating peak flow rate at different return periods. Virginia, for example, is separated into eight hydrologic regions in the VDOT Drainage Manual (VDOT, 2014). Each hydrologic region has regression equations based on the analysis of stream gage data in that region. These regression equations relate the size of a drainage area to peak flow rates for different return period storms.

River Cross-section Properties at Bridge Locations

Cross-section Profile. The cross-section profile at bridge locations can be estimated using the NHD Flowline feature class, a 200-year floodplain available from FEMA, and a digital elevation model (DEM). The first step is to snap each bridge to a NHD Flowline feature. Next, seven different cross-section lines are determined at each bridge location, one at the snapped bridge location and three in both the upstream and downstream directions. This is done to obtain average cross-section conditions near the bridge location. The steps for completing this are first to trace upstream on the flowline and place points on an equidistance interval (e.g., two meter

intervals between adjacent points) from the snapped bridge location. This distance can be set by the user, but most often will be determined by the DEM resolution. Then the same process is repeated in the downstream direction from the snapped bridge location. Lines perpendicular to the flowline are placed at each point and extend to some distance (e.g., 100m) beyond the boundary of the 200-year floodplain. This procedure has been automated as a script using the Python programming language and an example of the resulting cross-section lines is given in Figure 2. The set of lines perpendicular to the flowline at a given bridge location are used to determine the averaged river cross-section profile.

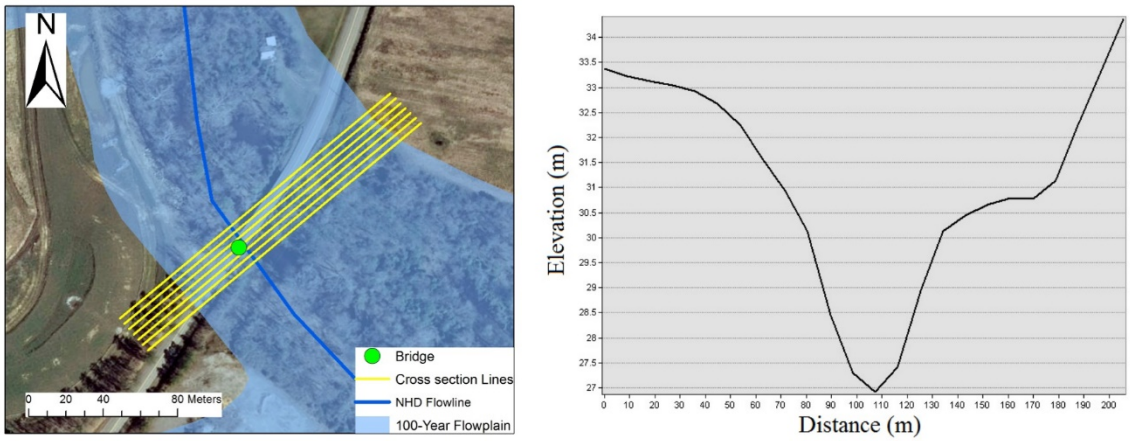

FIGURE 2. (a) Example of Identifying the River Cross-section at a Bridge Location; (b) Resulting Averaged River Cross-section Profile at the Bridge Location

High resolution DEM data is required to generate a cross-section profile at a bridge location. If more local data with higher resolution is not available, the National Elevation Dataset (NED) provided by USGS can be used for this purpose. The Geospatial Data Abstraction Library (GDAL) (http://www.gdal.org/) is a translator library for raster and vector geospatial data formats. The "ReadAsArray" tool in GDAL is used to sample values of the DEM raster along the

lines perpendicular to the Flowline feature using two steps. (1) Find the vertexes for each line and place a fixed number of points equidistant between each pair of vertexes. (2) For every point along the line, use the "ReadAsArray" tool in the GDAL library to read the elevation at that point from DEM. The array of elevations for each line is that line's cross-section profile. The bridge's cross-section profile is determined by averaging the cross-section profiles for the seven lines associate with the bridge.

Manning's Roughness Coefficient. The Manning's roughness coefficient (n) represents the frictional resistance to flows in channels and floodplains (McCuen, 1998). The National Land Cover Database (NLCD), which is commonly used in hydrologic models to assign Manning's roughness (Kalyanapu et al., 2009), is used in the method to estimate Manning's roughness at each river cross-section. The 2011 version of the NLCD contains 16 land cover classes and each land cover class is coded with a definition that describes the surface properties. Using the suggested values for land surface roughness from McCuen (1998), a Manning's roughness is assigned to each grid cell based on its code. For example, the assigned Manning's roughness for land use code 24 (developed, high intensity) is determined by an area weighted average where 80% of the area is assigned the value for concrete (0.013) and 20% is assigned the value for short grass (0.15), producing a weighted average roughness value of 0.040 (Kalyanapu et al., 2009). Using this strategy, the Manning's roughness values of all land cover types can be computed (Table 1) and then assigned to each grid cell. Then, using an approach similar to what was described earlier for generating the river cross-section profiles, GDAL is used to determine Manning's roughness values along each river cross-section.

TABLE 1. Manning's Roughness Coefficients for NLCD 2011 Land Cover Types (Kalyanapu et al., 2009)

Land Cover Code	Land Cover Description	Manning's n
11	Waterbody	0.035
21	Developed, open space	0.0404
22	Developed, low intensity	0.0678
23	Developed, medium intensity	0.0678
24	Developed, high intensity	0.0404
31	Barren land	0.0113
41	Deciduous forest	0.36
42	Evergreen forest	0.32
43	Mixed forest	0.4
52	Shrub/srcub	0.4
71	Grassland/herbaceous	0.368
81	Pasture/hay	0.325
82	Crop/vegetation	0.3228
90	Woody wetlands	0.086
95	Emergent herbaceous wetlands	0.1825

Channel Bed Slope. Channel slope at each bridge cross-section is obtained from the NHDPlusAttributes table in the NHD. The slope of the closest Flowline feature intersecting with each river cross section is assumed to represent the bottom channel slope of that river cross-section.

Estimating the Water Surface Elevation at Peak Flow for Bridges

The water surface elevation at peak flow for a bridge location is estimated using Manning's Equation (Equation 1) and the cross-section properties at that bridge location.

$$Q = \frac{1}{n} A R^{\frac{2}{3}} S^{\frac{1}{2}} \quad (1)$$

In Equation 1, Q (m^3/s) is flow rate, n is the Manning's roughness coefficient, A (m^2) is the cross-sectional area of flow, R (m) is the hydraulic radius, and S is the bed slope. The cross-sectional area and the hydraulic radius are functions of the water surface elevation (y). With the

cross-section properties found in the prior steps, Equation 1 can be solved for each bridge using an iterative process where the water surface elevation (y) is varied until the estimated peak flow rate matches the expected peak flow rate for a given return period.

The algorithm used to implement this procedure including all input and output variables is described in Figure 3. All input data are estimated using the approaches described in the prior subsections. *A (y, E)* is a function that calculates the cross-sectional area of flow for a given surface water level (*y*) and related cross-section profile (*E*). The function *R (y, E)* is used to compute the hydraulic radius for a given water surface level (*y*) and corresponding cross-section profile (*E*). Based on an array of Manning's roughness coefficients along the cross-section line, the function *n (y, N)* is applied to calculate the average Manning's roughness coefficient for the cross-section determined by a given surface water level (*y*). Finally, *Q (A, R, n, S)* is a function that uses Equation 1 to calculate flow rate. This algorithm was implemented as a script using the Python programming language to automate the process for all bridge locations in the study area.

```
Algorithm
    input:   QP, an array of peak flow rates for each return period
             S, channel bottom slope
             E, an array of elevation values along the cross-section line
             N, an array of Manning's roughness coefficients along the cross-section line
    output:  y, water surface elevation
    (Note: Qe is the flow rate calculated from Manning's equation)

    for each Q in QP do
        let Y be an array of surface water levels from 0 to bankfull with an interval of Δy

        for each y in Y do
            A := A(y, E)
            R := R(y, E)
            n := n(y, N)
            Qe := Q(A, R, n, S)
            Diff := abs[(Qe - Q)/Q]
            if Diff < threshold value (e.g., 0.1%) then
                y is a match for Q
            endif
        end for
        if length(y) > 1 then
            (Note: multiple matching y's)
            inform user about multiple matching y's
            select largest y as worst case
        else if number(y) = 0 then
            inform user no proper y found
        end if
    end for
    return y
```

FIGURE 3. Algorithm for Determining Surface Water Elevation at a Bridge Location for a Set of Peak Flow Rates Corresponding to Different Return Periods

EXAMPLE APPLICATION

The method was applied in an example application for a collection of 475 bridges located in the Hampton Roads region of Virginia. The application resulted in the identification of bridges at risk for overtopping due to storms with different return periods. This data was combined with

transportation data for each bridge to identify critical bridges within the transportation network that are vulnerable to overtopping.

Study Area

The study area for this research includes a portion of the Blackwater, Norttoway, and Meherrin River basins located within the VDOT Hampton Roads District (Figure 4). The study area covers approximately 4,592 km^2 of low-lying coastal plain. Surface elevation gently rises from east to west across the study area. The area reaches a maximum elevation of about 98 m above sea level along its western edge and drops to 0.3 m at the lowest point.

The bridge dataset (Figure 4) was provided by VDOT's Hampton Roads district. This dataset contains the deck elevation for each of the 475 bridges. There are 11 stream gages in this region maintained by the US Geological Survey (USGS) located mainly on higher order streams and not on smaller tributaries. As a result, most of the bridges in the study area are located on streams without gaging stations. Other geographic data used in the study include a NED 1/3 arc-second DEM, NLCD 2011, and floodplain maps and base flood elevations from FEMA. The DEM has a resolution of 9.2m x 9.2m after it was projected and the NLCD 2011 has a resolution of 30m x 30m. Higher resolution datasets, if available, could be used in place of these national-scale datasets in the analysis when applied to other study regions.

Both the USGS StreamStats and regression equations in VDOT drainage manual are used to estimate the peak flow rate at return periods of 5, 10, 25, 50, 100, and 200-year. The USGS StreamStats service for estimating peak flow rates in Virginia is based on two separate USGS reports. The first report (Austin 2011) contains regression equations for estimating the peak flow rate of a stream obtained by analyzing stream gage records from 1895 to 2007. The second report (Austin 2014) includes methods and equations for estimating peak streamflow in Virginia's

urban basins. The VDOT drainage manual adopted the outcome from a USGS report in 1995 (Bisese, 1995), which contains regression equations developed by analyzing stream gage record from 1895 to 1991. Thus, the USGS StreamStats regression equations are based on newer information (streamflow data up to 2007) compared to the VDOT regression equations, which only consider data up to 1991. The analyses presented in the following subsections are based on flow rate estimates from both methods to better understand their similarities and differences when used to estimate bridge overtopping.

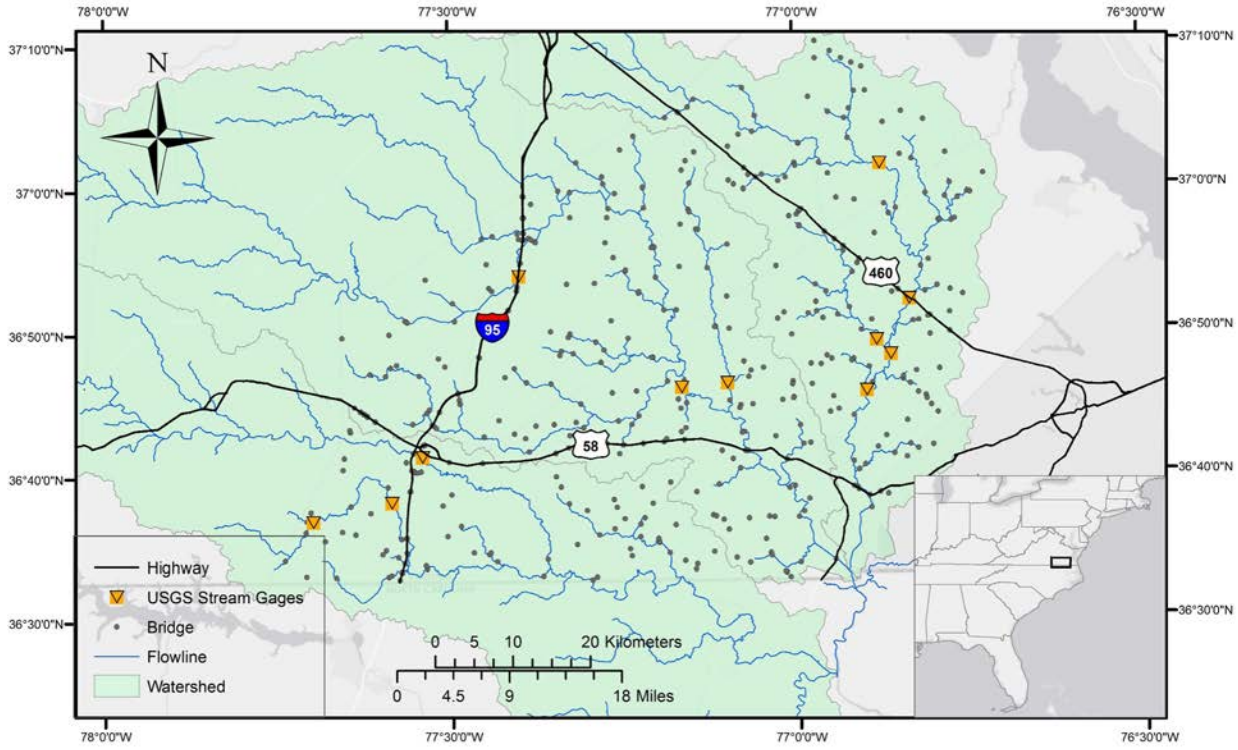

FIGURE 4. Study Area Including Bridges and USGS Stream Gages within a Portion of the Hampton Roads VDOT District

A dataset for Virginia roadways named "Annual Average Daily Traffic (AADT) volumes with Vehicle Classification Data" was obtained from the VDOT website (http://www.virginiadot.org/info/ct-trafficcounts.asp). This dataset includes road functional

classification and AADT volumes for the years 1985 to 2014. The study area includes major roadways, such as Interstate 95, US Route 58, and US Route 460 (Figure 4) with approximated AADT of 40,000, 14,000, and 10,000, respectively. The data were clipped to the study area boundary to extract information for only the region being studied. The intersect tool in ArcGIS was used to determine the AADT values for each bridge.

Results and Discussion

Bridge Flooding Risk. Table 2 presents the number of bridges estimated to be overtopped by 5, 10, 25, 50, 100, and 200-year flooding events. The number of bridges overtopped when estimated using USGS StreamStats peak flow rates is typically higher than when using the VDOT drainage manual peak flow rates. Using the VDOT peak flow rate estimates, 22 (4.6%) of the bridges could be overtopped by 5-year flood. Using the USGS StreamStats peak flow rate estimates results in the same 22 bridges being overtopped by a 5-year flood plus one additional bridge not identified when using VDOT peak flow rates. The number of overtopped bridges estimated by StreamStats and VDOT regression equations have generally increasing differences as the storm return period increases. For example, the number of bridges overtopped by a 10-year storm are 28 (5.9%) and 30 (6.3%) for the VDOT and USGS peak flow rate estimates, respectively. These numbers increase to 36 (7.6%, VDOT Drainage Manual) and 42 (8.8%, USGS StreamStats) for a 25-year flooding event. For a 100-year storm, the peak flow rate estimate from USGS StreamStats results in 21 more bridges overtopped compared to VDOT peak flow rate estimates.

The differences between bridge overtopping estimates generated using the USGS StreamStats and VDOT drainage manual approaches is a result of the peak discharge generated

from these two approaches. The USGS derived peak discharge is always higher than the VDOT peak discharge when averaged over all bridges within the study area (Figure 5). The difference between the two average peak discharges also increases for storms with higher return periods. Given that all other variables with the approach are constant and only the peak discharge changes, this difference shown in Figure 5 explains the difference in the number of overtopped bridges estimated by these two methods shown in Table 2. As stated earlier, the USGS regression is based on more recent streamflow data (up to 2007) compared to the VDOT regression equation, which only considered streamflow data up to 1991. This difference likely accounts for the observed differences in discharge shown in Figure 5.

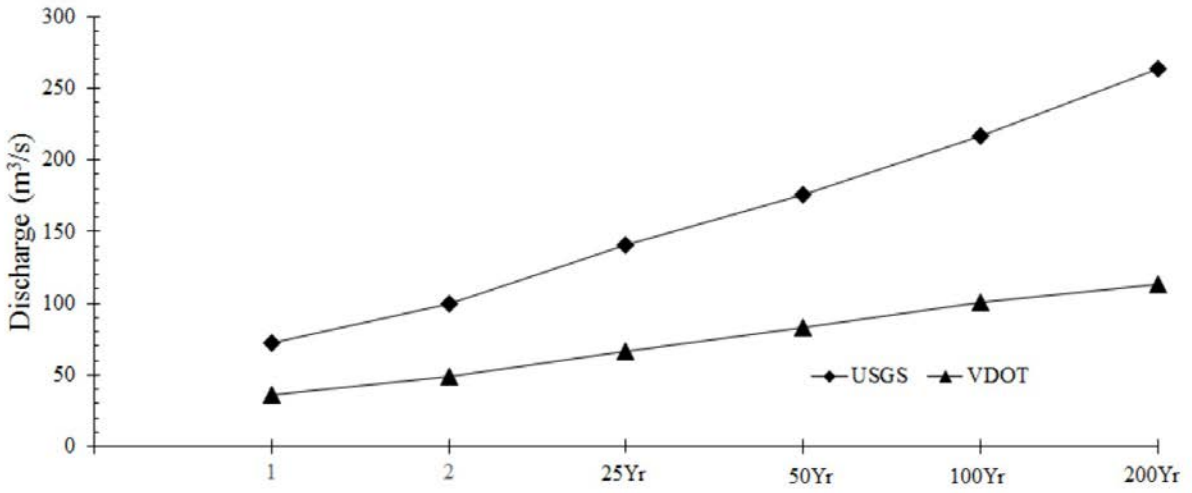

Figure 5. Average Peak Flow Rate Across All Bridges within the Study Area for Storms with Different Return Periods

Table 2 shows the number of bridges estimated by both methods to be overtopped in the "Intersect" row. This intersection count shows that, in general, bridges identified when using the estimates from the VDOT Drainage Manual regression equations are also contained in the estimates when using USGS StreamStats. The "Union" row in Table 2 gives the number of

bridges at risk of overtopping based on either the VDOT or USGS peak flow estimates. This union count gives the number of bridges estimated to be vulnerable to overtopping based on either the USGS or VDOT generated peak flow estimates. For the 5, 10, and 100-year return periods, the union counts are identical to the number of bridges identified to be overtopped using the USGS StreamStats method. For the 25, 50, and 200-year return periods, the union counts are within two of the USGS StreamStats counts. This means that one to two bridges for each of these return periods were identified to be vulnerable to overtopping using the USGS StreamStats method, but not identified to be vulnerable to overtopping when using the VDOT Drainage Manual method.

TABLE 2. Number and Percentage of Bridges Vulnerable to Overtopping by Flooding Events with Different Return Periods

Method	Flood Risk											
	5-year		10-year		25-year		50-year		100-year		200-year	
USGS StreamStats	23	4.8%	30	6.3%	42	8.8%	60	12.6%	83	17.5%	93	19.6%
VDOT Drainage Manual	22	4.6%	28	5.9%	36	7.6%	49	10.3%	62	13.1%	73	15.4%
Intersect	22		28		34		47		62		72	
Union	23		30		44		62		83		94	

Figure 6 gives the geographic location of bridges identified to be overtopped by storm events with different return periods when using the (a) USGS StreamStats and (b) VDOT regression equations. The streamline used in Figure 6 is a simplified version of the NHD Flowline feature class. The highest stream order in the study area according to the NHD is five. The Figure shows that bridges overtopped by small flooding events are located mainly on lower order streams. For example, all bridges overtopped by a 5-year flooding event as estimated by both methods are located on streams with order no greater than 2. For a 10-year flooding event, about 27% (USGS StreamStats) and 39% (VDOT) of vulnerable bridges are located on streams

of order 3, and the rest are on streams of order 1 or 2. As might be expected, for larger and, therefore, less frequently reoccurring storm events, some bridges on higher order streams could be overtopped. For example, among all bridges vulnerable to 100-year flooding event estimated by USGS StreamStats method, there are 7 (8%) bridges located on order 4 streams and 6 (7%) on order 5 streams. For the same case using the VDOT method, there are 5 (8%) bridges on order 4 streams and the same number of bridges on order 5 streams. In Figure 6, small gray dots represent the 381 (80%) bridges not predicted to be overtopped by even a 200-year flooding event using either the USGS StreamStats or VDOT methods. Among those bridges, 162 (34%) do not cross waterbodies (many presumably cross other roads or rail lines) and the remaining 219 (46%) do cross waterbodies but are not estimated to be overtopped by 200-year flooding event.

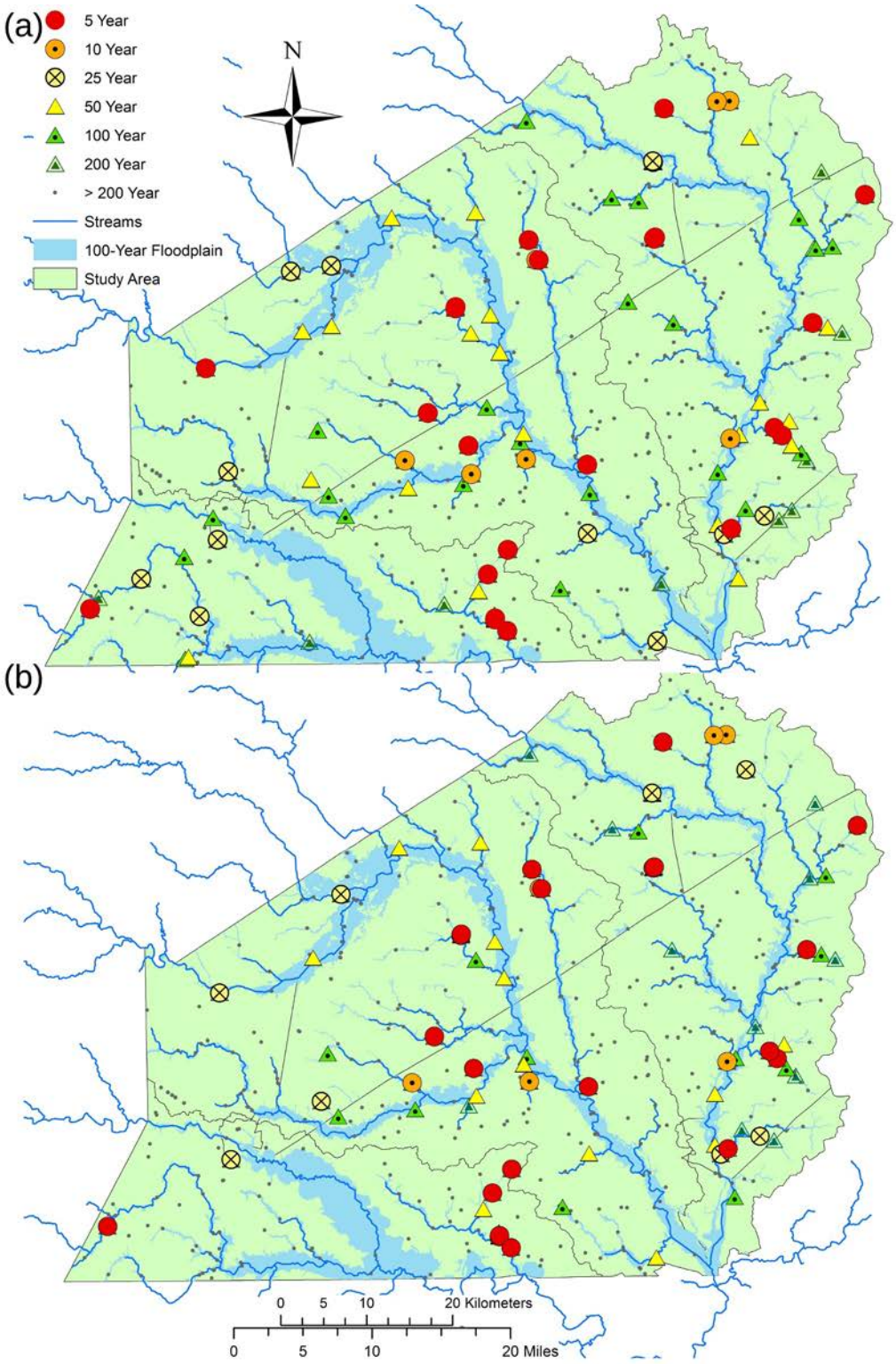

FIGURE 6. Bridges Overtopped by Floods with Different Return Periods Using Peak Flow Rates Estimated from (a) USGS StreamStats and (b) VDOT Drainage Manual Regression Equations

Model Evaluation. The results of this analysis were evaluated against water surface elevation data available through the FEMA flood mapping program. FEMA performs flood modeling in order to generate 100-year flood maps used for flood insurance purposes. Only certain portions of major rivers within the study region (Figure 7) were modeled by FEMA using a 1-D hydrodynamic model to estimate the peak water surface elevation due to a 100-year flooding event. Developing and applying these models are time and resource intensive and not practical to implement across all streams within the study region. These peak water surface elevation estimates generated using the FEMA models were compared to the water surface elevation estimates generated through this analysis for all bridges within the study region.

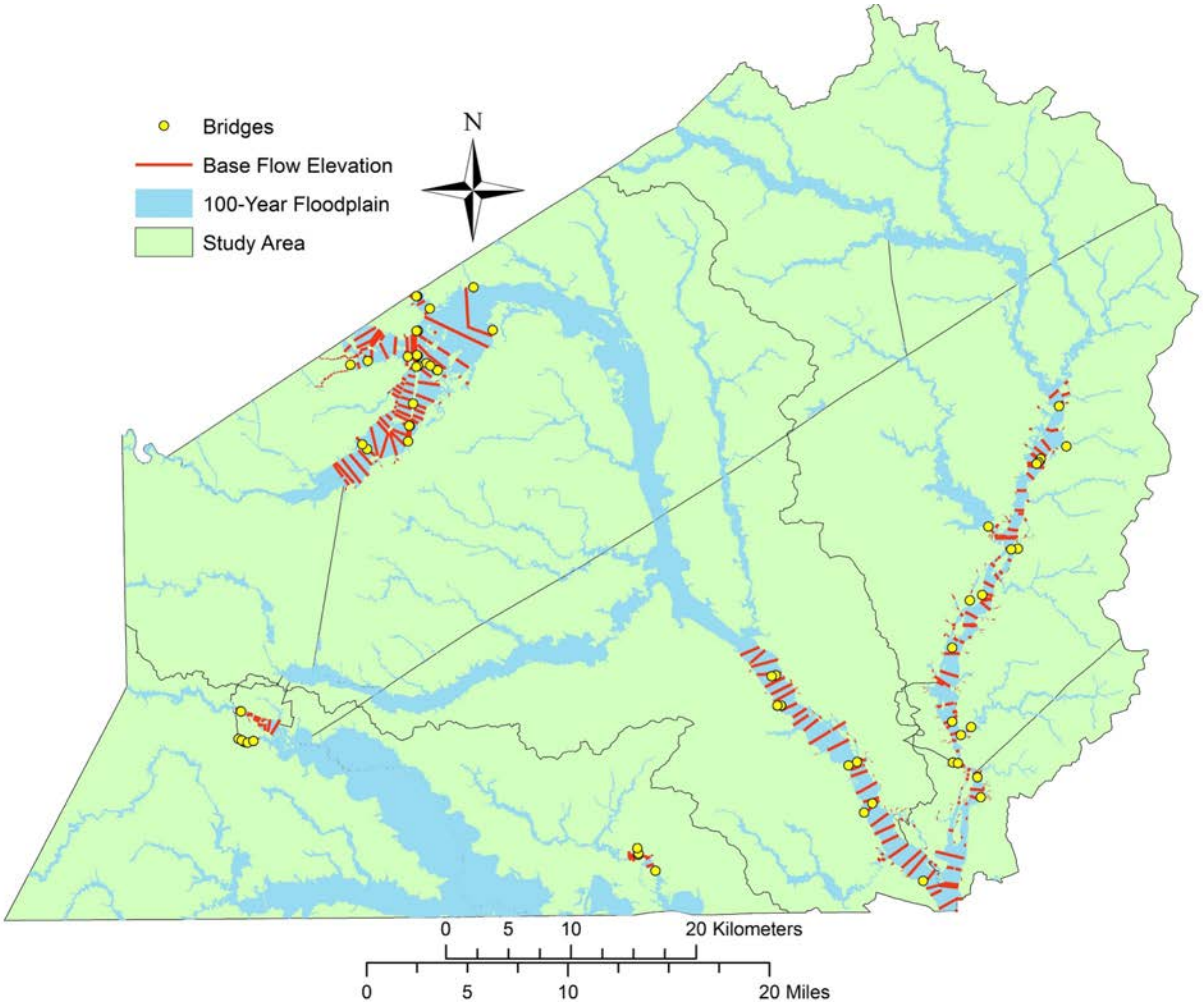

FIGURE 7. FEMA 100-year Storm Water Surface Elevation Used for Verifying Water Surface Elevation Estimates Generated Using USGS Steamstats and VDOT Regression Equations.

Figure 8 plots the FEMA 100-year storm water depth with against the water depth estimates calculated using the screening tool along with the USGS StreamStats and VDOT regression equations. The linear trendline in both cases are parallel to, but slightly above, a 1:1 line. This means peak flow elevation estimates from the screening tool are generally in agreement with, although potentially slightly below, those generated through the more sophisticated FEMA modeling efforts. The Root-Mean-Square Error (RMSE) was used to quantify differences between estimates from this method and estimates generated by FEMA (i.e., deviations from the 1:1 line in Figure 8). RMSE can be calculated as

$$RMSE = \sqrt{\frac{\sum_{i=1}^{N}\left(\widehat{D}_i - D_i\right)^2}{N}} \quad (2)$$

where, $\widehat{D}_i$ is the estimated water depth (m) using USGS StreamStats or VDOT method at bridge i, D_i is the peak water depth (m) provided by FEMA, and N is the total number of bridges.

The RMSE for the USGS StreamStats water depths is 1.84 m compared to 2.08 m for VDOT water depths. Thus, the USGS StreamStats is a slightly better fit with the FEMA estimations, which may be due to it using more recent streamflow data.

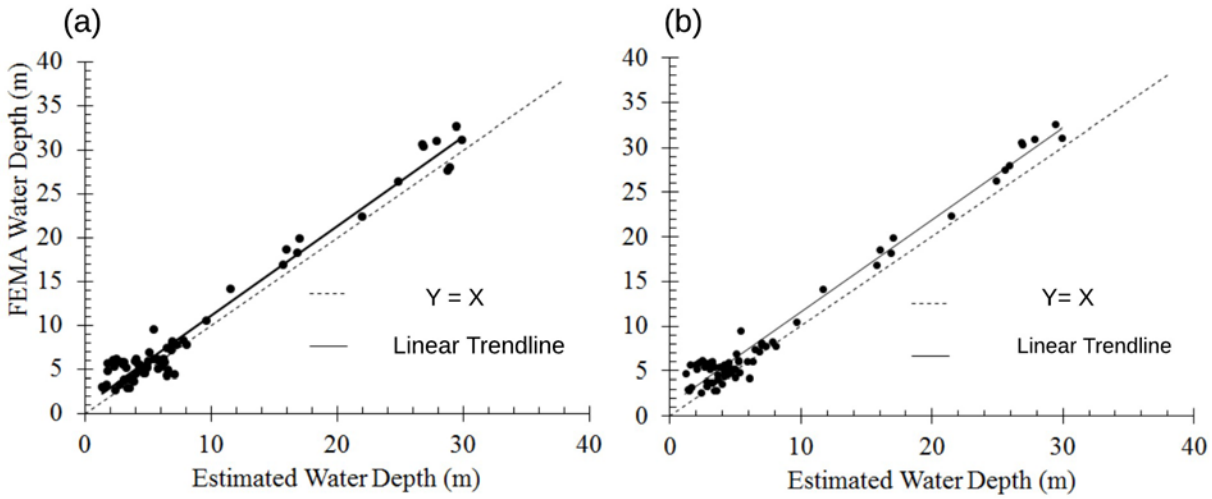

FIGURE 8. Water Depth Estimated Using the Detailed FEMA Flood Models Compared to Water Depth Estimated Using (a) the USGS StreamStats and (b) the VDOT Regression Equations **Flood Risk and Transportation Network.** The bridges estimated to be overtopped using the screening tool and either USGS or VDOT peak flow (e.g., what we referred to as the union results earlier) were combined with traffic information for each bridge to identify high traffic volume bridges that are also vulnerable to overtopping. Table 3 presents the number and percentage of vulnerable bridges within different annual average daily traffic volume (AADT) classes, and Figure 9 shows these data geographically. The analysis suggests that many of the bridges that would be overtopped by smaller flooding events (e.g., 5-year flood) do not carry significant traffic volume (AADT < 500). However, there are some bridges that carry moderate traffic volume (AADT > 1000) that, based on this analysis, could be overtopped by 5, 10, or 25-year flooding events. There are three bridges carrying AADT from 1000 to 5000 that, based on this screening analysis, may be overtopped by 5-year flooding event. Several highway bridges with heavier traffic volume (AADT > 5000) may be vulnerable to larger flood events (50 year or above). These bridges carrying heavier traffic volume and at risk of flooding are further investigated later in this section to better understand their potential risk due to overtopping.

TABLE 3. Number and Percentage of Overtopped Bridges within Different Annual Average Daily Traffic (AADT) Classes

AADT	Total Bridge	Flood Risk					
		5-year	10-year	25-year	50-year	100-year	200-year
< 100	84	6 (7%)	9 (11%)	12 (14%)	15 (18%)	17 (20%)	19 (23%)
100 - 500	183	11 (6%)	15 (8%)	23 (13%)	30 (16%)	43 (23%)	48 (26%)
500 - 1000	141	3 (2%)	3 (2%)	5 (4%)	9 (6%)	11 (8%)	14 (10%)
1000 - 5000	253	3 (1%)	3 (1%)	4 (2%)	6 (2%)	9 (4%)	10 (4%)
> 5000	222				2 (1%)	3 (1%)	3 (1%)
Sum	475	23	30	44	62	83	94

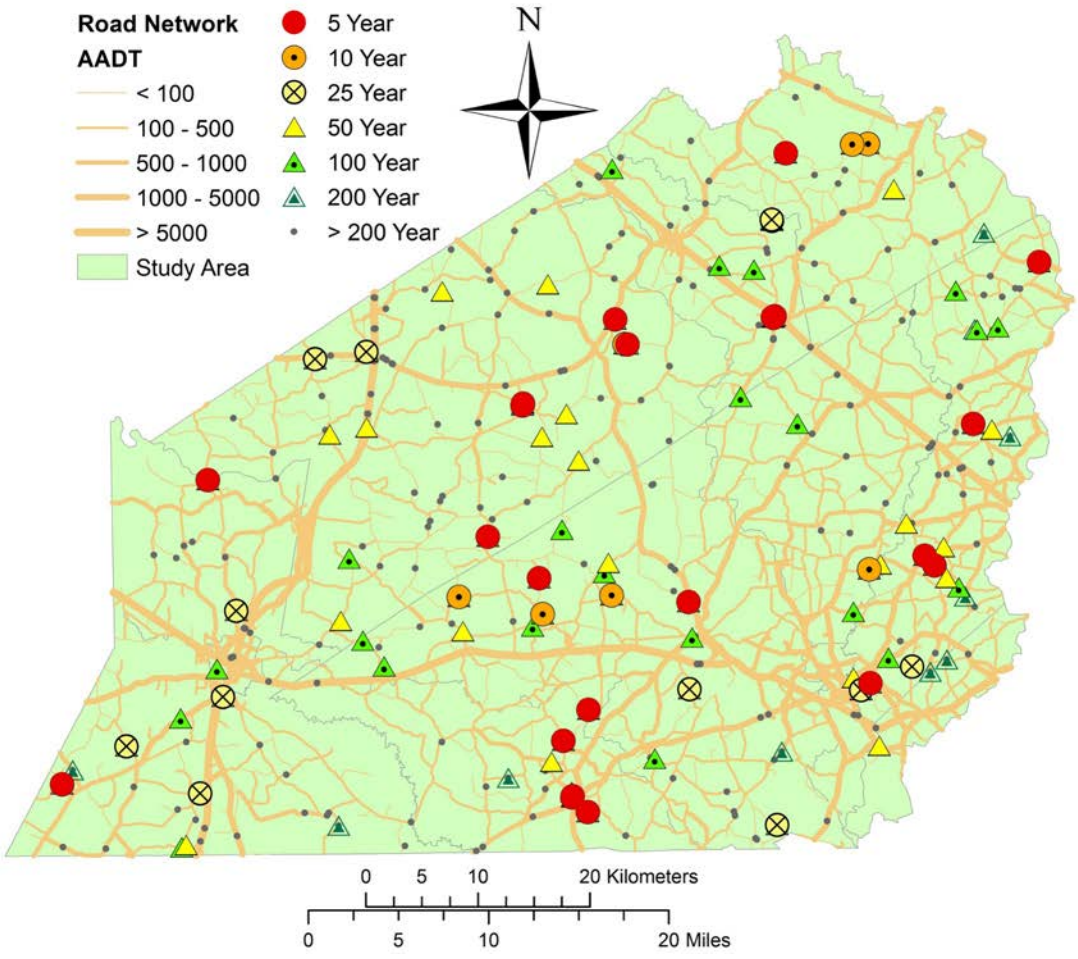

FIGURE 9. Annual Average Daily Traffic of Overtopped Bridges Identified by Combining Estimates from USGS StreamStats and Regression Equations in VDOT Drainage Manual

Flood risk was also compared to road functional classifications given that some roads with lower traffic volumes may still be important links within the transportation network. The functional classification of roads for each bridge is available in the National Bridge Inventory (NBI) within the field named Functional Classification of Inventory Route. Organizing the flood risks according to functional classifications shows that very few Interstate, Freeway/Expressway, and even Minor Arterial bridges would be overtopped by a 200 year stors (Table 4). The majority of bridges impacted by such a storm are on smaller Collector and Local roads, and some of these bridges would be overtopped by more frequently occurring storms as well. A greater percentage of Local roads are estimated to be overtopped compared to other road classes for all storm return periods, as expected.

TABLE 4. Number and Percentage of Overtopped Bridges by Different Road Functional Classifications

Road Class	Total Bridge	Flood Risk					
		5-year	10-year	25-year	50-year	100-year	200-year
Interstate	27				1 (4%)	2 (7%)	2 (7%)
Freeway/ Expressway	27				1 (4%)	1 (4%)	1 (4%)
Minor Arterial	21				1 (5%)	2 (10%)	2 (10%)
Collector	139	7 (5%)	7 (5%)	13 (9%)	18 (13%)	22 (16%)	25 (18%)
Local	261	16 (6%)	23 (9%)	31 (12%)	41 (16%)	56 (21%)	64 (25%)
Sum	475	23	30	44	62	83	94

The bridges on Interstates and Freeway/Expressway road classes vulnerable to being overtopped were further analyzed to understand their specific conditions and context (Figure 10). One Interstate bridge (Figure 10-A), one Freeway/Expressway bridge (Figure 10-B), and one Minor Arterial bridge (Figure 10-C) were identified to be vulnerable to a 50-year or greater storm event. Another Interstate bridge (Figure 10-D) and Minor Arterial bridge (Figure 10-E)

were estimated to be vulnerable to a 100-year or greater storm events. Bridges A and E appear to be crossing smaller tributaries that are not part of the NHD Flowline feature dataset, but were within the flood plain of a larger nearby river 285m away in the case of Bridge A and 381m away in the case of Bridge B. Because these small tributaries are not part of the NHD Flowline feature dataset, the tool snapped these bridges to the nearby main branch of the river. The tributaries these bridges are over could reach the estimated peak water levels due to backing up of water from the main branch, given the proximity of these tributaries to the main branch. Thus, the prediction that these bridges are vulnerable to flooding may still be a valid concern and further analysis is warranted. Bridge D was is 435m downstream of a reservoir, and because reservoirs are not automatically accounted for in the current version of the screening tool, it is unlikely that this bridge would experience overtopping for a 100-yr event. Finally, Bridges B and C do not appear to have any obvious deterrents to overtopping and should be explored further for their potential risk to overtopping.

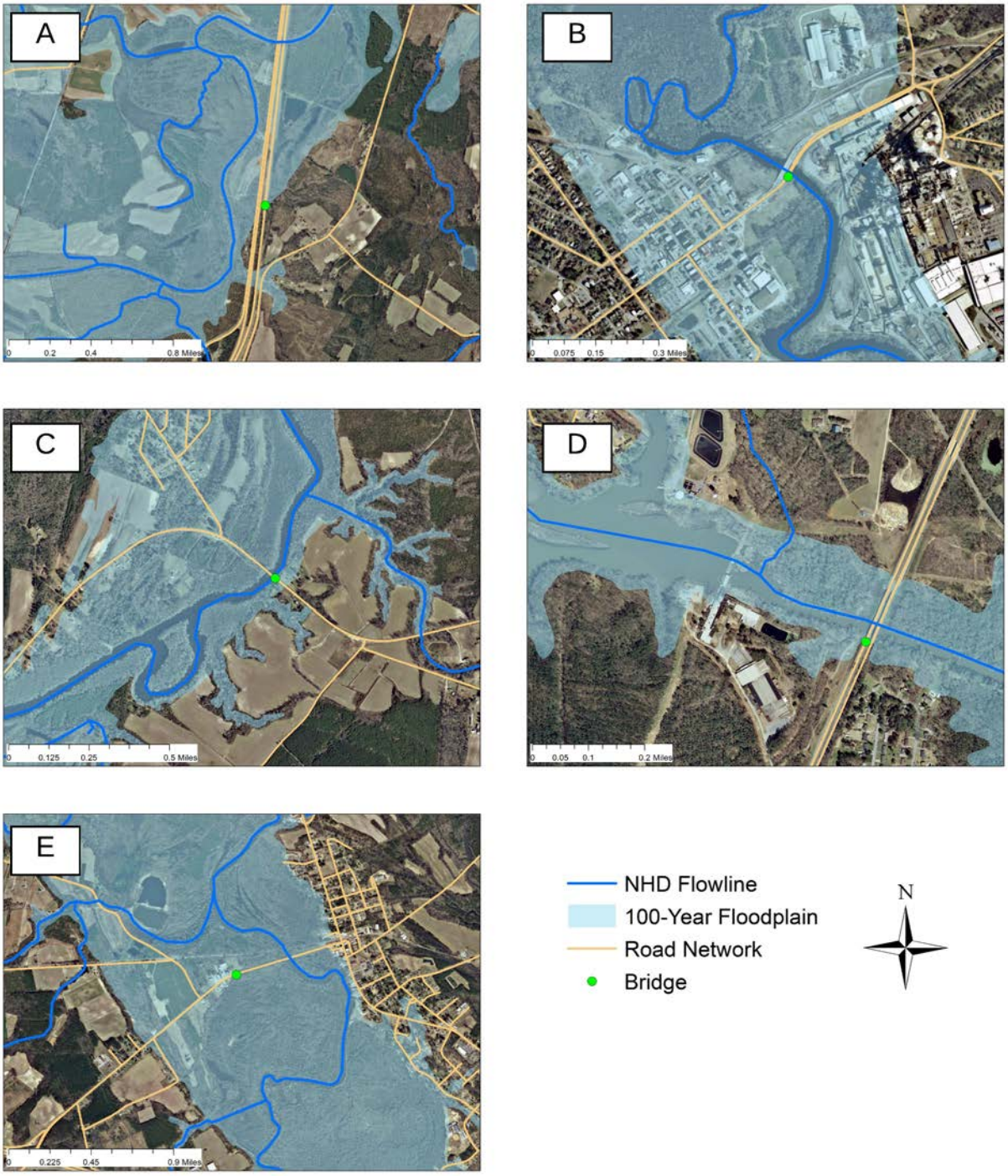

Figure 10. Location of Major Road Bridges Identified to be Potentially Vulnerable to Overtopping for a 100 year or great flooding event

In the National Bridge Inventory (NBI), overtopping frequency is stored in the Waterway Adequacy field and is classified into ten functional classifications (FHWA, 1995). These classifications are grouped into four overtopping frequency categories: (1) Remote, meaning greater than 100 years; (2) Slight, meaning 11 to 100 years; (3) Occasional, meaning 3 to 10 years; (4) Frequent, meaning less than 3 years. Because a 5-year storm was the most frequently occurring storm analyzed in this study, there is no equivalent between the results of this study and the NBI "frequent" category. Bridges identified in this study to be vulnerable to overtopping for a 5 or 10-year storm were compared to the NBI "occasional" category, while bridges identified to be vulnerable to 25, 50, and 100-year storms were compared to the NBI "slight" category. Bridges vulnerable to a 200 or greater year storm event were compared to the NBI "remote" category.

The results of this comparison to the NBI Waterway Adequacy field show that this method resulted in many of the bridges being placed into a "remote" category compared to the "slight" category (Table 5). Bridges vulnerable to overtopping for a 100-year storm are on the border between these two categories, and this would explain a fraction of the differences as 83 bridges were identified as being vulnerable to overtopping for a 100-year storm. The "Intersect" row in Table 5 gives the number of bridges classified in the same category by both the NBI and the screening tool. This means that, of the 80 bridges classified as being overtopped occasionally by the NBI, only eight of these bridges were classified to be in the same category by the screening tool. However, the screening tool did identify 20 of the 22 bridges identified within the NBI as having a remote chance of being overtopped. The NBI relies on the inspector's judgment based on an assessment of the bridge location to populate the Waterway Adequacy field. This can be very challenging to do accurately given that risk of overtopping requires hydrologic

understanding of the watershed draining to the bridge location. The method described in this paper could be further refined and then implemented nationally to provide a suggested Waterway Adequacy category to bridge inspectors, that they could then adjust as needed based on their own expert judgment.

TABLE 5. Number of Bridges with Different Frequencies of Overtopping Based on the Classification in the Waterway Adequacy Field in National Bridge Inventory (NBI)

	Frequent	Occasional	Slight	Remote
NBI	0	80	373	22
Estimated	N/A	30	53	392
Intersect		8	39	20

CONCLUSIONS

The primary objective of this paper was to develop a methodology for screening a large collection of bridges to determine their risk of overtopping due to flooding events of varying return periods. The method makes use of publicly available datasets, tools, and regression equations to evaluate bridge vulnerability to flooding over a large spatial scale. The method was applied for a portion of the Hampton Roads region in Virginia that contains 475 bridges. In the example application, both USGS StreamStats and regional regression equations in the VDOT Drainage Manual were applied to estimate peak flow rates. These peak flow rate estimates were used with other public databases, such as NLCD 2011, NHDPlus, FEMA floodplain map, and NED to estimate the corresponding water surface elevation at the bridge locations. By comparing the deck elevation, which was obtained from the bridge owners, with the estimated water surface elevation, it was possible to determine if each bridge in the region would be overtopped for a flood event with a given return period.

The primary benefit of the method is that it provides a quick and inexpensive approach for estimating the overtopping risk of many existing bridges. The method leverages nationally available geospatial datasets, simple hydrologic and hydraulic principles, and geospatial analysis to estimate overtopping, whereas more intensive (but also more accurate) methods would require building, calibrating, and validating detailed hydrologic and hydraulic models. It is important to have lower cost screening methods because changing environmental and land use conditions may result in streamflow conditions not anticipated when the bridge was designed. Conducting detailed hydrologic and hydraulic analyses for all bridges will likely be cost prohibitive; therefore, this method is designed as a screening tool to direct detailed analyses to certain bridges identified through the screening analysis. It is envisioned that this analysis could be used as part of ongoing bridge maintenance activities. For example, the National Bridge Inventory (NBI) Waterway Adequacy field requires knowledge of the risk that a bridge will be overtopped. This method could assist in maintaining the Waterway Adequacy field as new data become available.

With the exception of bridge deck heights, all other data required by the method are available from public and nationally available datasets. Thus, this method could be used for other regions of the country as well, provided that bridge deck heights are known. The example application used a relatively coarse resolution DEM and land use data provided through federal data providers. If surveyed cross-section profiles at bridge locations are available, then this data could be used in the tool to derive more accurate cross-section profiles. Likewise, if a higher resolution DEM or land use data are available for the study area from local data providers, then these data can be easily inserted into the method. Future research exploring the sensitivity of the method to cross-sectional data derived from different sources (survey vs. DEMs of increasing

resolution), would help in understanding the tradeoff in accuracy introduced as more coarse elevation data is used for deriving cross section profiles.

Two other general approaches for further advancing this work are (1) building a user-friend tool implementing the method and (2) improving the identification of critical bridges within the network under various bridge overtopping scenarios. User-friendly software could more fully automate the data processing steps, which through this work were only semi-automated as a set of Python scripts. Added functionality could also allow users to insert known cross-section properties for select bridges that could be combined with DEM-generated cross-section properties for other bridges. This would allow both complete coverage of all bridges within a region and the ability to use the best available information for each bridge. Future research could also more fully explore the process by which critical bridges are identified within the network. Rather than simply looking at traffic counts or road functional classifications as a measure of how critical a bridge is in the network, future work could look at how trips would be impacted if multiple bridges failed simultaneously due to overtopping.

ACKNOWLEDGEMENTS

The authors wish to acknowledge support from the Mid-Atlantic Transportation Sustainability (MATS) University Transportation Center (UTC) for sponsoring this research. Andrew B. Scott and John H. Matthews of VDOT provided the bridge deck height data used in the analysis and offered very helpful comments on the research methodology and results.

LITERATURE CITED

AASHTO, 2012. *ASSHTO LRFD bridge design specifications*. American Association of State Highway and Transportation Officials, Washington, DC. ISBN: 978-1-56051-523-4

Austin, S.H., 2014, *Methods and equations for estimating peak streamflow per square mile in Virginia's urban basins*: USGS Report 2014–5090

Austin, S.H., J.L. Krstolic, and U. Wiegand, 2011. Peak-Flow Characteristics of Virginia Streams.: USGS Report 2011–5144

Bala, S.K., M.M. Hoque, and S.M.U. Ahmed, 2005. Failure of a Bridge due to Flood in Bangladesh - A Case Study. *Journal of Civil and Environmental Engineering* 1(1):38–44.

Bisese, J.A., 1995. Methods for Estimating the Magnitude and Frequency of Peak Discharges of Rural, Unregulated Streams in Virginia. USGS Water Resources Investigations Report 94-4148.

Bonnin, G.M., K. Maitaria, and M. Yekta, 2011. Trends in Rainfall Exceedances in the Observed Record in Selected Areas of the United States. *Journal of the American Water Resources Association* (JAWRA) 47(6):1173–1182. DOI: 10.1111/j.1752-1688.2011.00603.x

Bouska, K.L. and T.J. Stoebner, 2015. Characterizing Geomorphic Change from Anthropogenic Disturbances to Inform Restoration in the Upper Cache River, Illinois. *Journal of the American Water Resources Association* (JAWRA) 51 (3):734–745. DOI: 10.1111/jawr.12266

Cigada, A., S. Malavasi, and M. Vanali, 2001. Direct Force Measurements on a Submerged Bridge Model. Transactions on the Built Environment 56:305–314.

Collins, M.J., 2009. Evidence for Changing Flood Risk in New England since the Late 20th Century. *Journal of the American Water Resources Association* (JAWRA) 45 (2):279–290. DOI: 10.1111/j.1752-1688.2008.00277.x

Deng, L. and C.S. Cai, 2010. Bridge Scour: Prediction, Modeling, Monitoring, and Countermeasures — Review. *Practice Periodical on Structural Design and Construction* 15 (2):125–134. DOI: 10.1061/(ASCE)SC.1943-5576.0000041

FHWA, 1995. Recording and Coding Guide for the Structure Inventory and Appraisal of the Nation's Bridges. U.S. Department of Transportation Federal Highway Administration Report FHWA-PD-96-001. http://www.fhwa.dot.gov/bridge/mtguide.pdf.

FHWA, 2012. Bridge Inspector's Reference Manual. U.S. Department of Transportation Federal Highway Administration Report FHWA-NHI-12-049. https://www.fhwa.dot.gov/bridge/nbis/pubs/nhi12049.pdf.

Guo, J., 2011. Time-Dependent Clear-Water Scour for Submerged Bridge Flows. Journal of Hydraulic Research 49:744–749. DOI: 10.1080/00221686.2011.616364

Hong, S.H. and T.W. Strum, 2010. Physical Modeling of Abutment Scour for Overtopping, Submerged Orifice, and Free Surface Flows. In: *International Conference on Scour and Erosion*, Burns, S. E., Bhatia, S. K., Avila, C. M. C., and Hunt, B. E. (Editor). American Society of Civil Engineers, San Francisco, CA, pp. 590–598.

Hu, B., H. Wang, Z. Yang, and X. Sun (2011). Temporal and spatial variations of sediment rating curves in the Changjiang (Yangtze River) basin and their implications. Quaternary International, 230(1), 34-43.

Hunt, B.E., 2005. Scour Monitoring Programs for Bridge Health. *Journal of the Transportation Research Board*:531–536. DOI: http://dx.doi.org/10.3141/trr.11s.xv8n83138r22j22k

Jain, S.C. and E.E. Fischer, 1979. Scour Around Circular Bridge Piers at High Froude Numbers. Iowa Institute of Hydraulic Research Report 220. http://www.iihr.uiowa.edu/wp-content/uploads/2013/11/IIHR220.pdf

Kalyanapu, A.J., S.J. Burian, and T.N. McPherson, 2009. Effect of Land Use-Based Surface Roughness on Hydrologic Model Output. *Journal of Spatial Hydrology* 9 (2):51–71. ISSN: 15304736

Kara, S., T. Stoesser, T.W. Sturm, and S. Mulahasan, 2015. Flow Dynamics through a Submerged Bridge Opening with Overtopping. Journal of Hydraulic Research 53:186–195. DOI: 10.1080/00221686.2014.967821

Khelifa, A., L.A. Garrow, M. Higgins, and M. Meyer, 2013. Impacts of Climate Change on Scour-Vulnerable Bridges: Assessment Based on HYRISK. *Journal of Infrastructure Systems* 19 (2):138–146. DOI: 10.15414/raae.2013.16.02.24-39

Lee, G.C., S.B. Mohan, C. Huang, and B.N. Fard, 2013. A Study of U.S. Bridge Failure (1980-2012). Earthquake Engineering to Extreme Events Report MCEER-13-0008. https://mceer.buffalo.edu/pdf/report/13-0008.pdf

Lee, T.L., D.S. Jeng, G.H. Zhang, and J.H. Hong, 2007. Neural Network Modeling for Estimation of Scour Depth around Bridge Piers. *Journal of Hydrodynamics* 19 (3):378–386. DOI: 10.1016/S1001-6058(07)60073-0

Li, L.Q., X.X. Lu, and Z.Y. Chen, 2007. River channel change during the last 50 years in the middle Yangtze River, the Jianli reach. *Geomorphology*. 85: 185-196. DOI: 10.1016/j.geomorph.2006.03.035.

Loaiciga, H.A., 2001. Flood Damages in Changing Floodplains: A Forensic-Hydrologic Case Study. *Journal of the American Water Resources Association* (JAWRA) 37 (2):467–478.

Malavasi, S., M. Riva, M. Vanali, and E. Larcan, 2001. Hydrodynamic Forces on a Submerged Bridge. Transactions on the Built Environment 56:45–54.

McCuen, R.H., 1998. Hydrologic Analysis and Design. Pearson Education, Upper Saddle River, New Jersey. ISBN: 9786468600

MDOT, 2006. Michigan Department of Transportation Drainage Manual. http://www.michigan.gov/stormwatermgt/0,1607,7-205--93193--,00.html

Melville, B.W., 1992. Local Scour at Bridge Abutments. *Journal of Hydraulic Engineering* 118 (4):615–631. DOI: 10.1680/iicep.1989.2004

Melville, B.W. and S.E. Coleman, 2000. Bridge Scour. Water Resources Publications, Auckland, New Zealand. ISBN: 1-887 201-18-1

MnDOT, 2000. Minnesota Department of Transportation Drainage Manual. http://www.dot.state.mn.us/bridge/hydraulics/drainagemanual.html

Newton, D.W. and J.C. Herrin, 1982. Assessment of Commonly Used Methods of Estimating Flood Frequency. *Transportation Research Record*:10–30.

Okeil, A.M. and C.S. Cai, 2008. Survey of Short- and Medium-Span Bridge Damage Induced by Hurricane Katrina. *Journal of Bridge Engineering* 13 (4):377–387. DOI: 10.1061/(ASCE)1084-0702(2008)13:4(377)

Padgett, J., R. DesRoches, B. Nielson, M. Yashinsky, O.-S. Kwon, N. Burdette, and E. Tavera, 2008. Bridge Damage and Repair Costs from Hurricane Katrina. *Journal of Bridge Engineering* 13:6–14.

Park, I., J. Lee, and W. Cho, 2004. Assessment of Bridge Scour and Riverbed Variation by a Ground Penetrating Radar. Tenth Iiitermtional Conference on Ground Penetrating Radar. Delft, The Netherlands 13(1), pp. 411–414.

Parola, A.C., D.J. Hagerty, and S. Kamojjala, 1998. Highway Infrastructure Damage Caused by the 1993 Upper Mississippi River Basin Flooding. National Cooperative Highway Research Program Report: 417. http://onlinepubs.trb.org/onlinepubs/nchrp/nchrp_rpt_417.pdf

Richardson, J.E. and V.G. Panchan, 1998. Three-Dimensional Simulation of Scour-Inducing Flow at Bridge Piers. *Journal of Hydraulic Engineering* 124 (5):530–540. DOI: 10.1061/(ASCE)0733-9429(1998)

Shan, H., Z. Xie, C. Bojanowski, O. Suaznabar, S. Lottes, J. Shen, and K. Kerenyi, 2012. Submerged Flow Bridge Scour under Clear Water Conditions. Report of US Federal Highway Administration: FHWA-HRT-12-034. Washington, D.C.Tucker, G. and R. Slingerland, 1997. Drainage basin responses to climate change. *Water Resources Research.* 33 (8): 2031-2047. DOI: 10.1029/97WR00409.

VDOT, 2014. Virginia Department of Transportation Drainage Manual. http://www.virginiadot.org/business/locdes/hydra-drainage-manual.asp

Wardhana, K. and F.C. Hadipriono, 2003. Analysis of Recent Bridge Failures in the United States. *Journal of Performance of Constructed Facilities* 17 (3):144–150. DOI: 10.1061/(ASCE)0887-3828(2003)

White, D.J., P.K.R. Vennapusa, and D.K. Miller, 2013. Western Iowa Missouri River Flooding — Geo-Infrastructure Damage Assessment. Iowa Highway Research Board Report: TR-638. http://www.intrans.iastate.edu/research/documents/research-reports/western_iowa_flood_damage_w_cvr.pdf

WSDOT, 2015. Washington State Department of Transportation Hydraulics Manual. http://www.wsdot.wa.gov/publications/manuals/m23-03.htm

Yang, S.L, Q.Y. Zhao, and I.M. Belkin (2002). Temporal Variation in the Sediment Load of the Yangtze River and the Influences of Human Activities. *Journal of Hydrology* 263(1), 56-71.

Yang, T., Q. Shao, Z. C. Hao, X. Chen, Z. Zhang, C. Y. Xu, and L. Sun (2010). Regional frequency analysis and spatio-temporal pattern characterization of rainfall extremes in the Pearl River Basin, China. *Journal of Hydrology* 380(3), 386-405.

Zounemat-Kermani, M., A.-A. Beheshti, B. Ataie-Ashtiani, and S.-R. Sabbagh-Yazdi, 2009. Estimation of Current-Induced Scour Depth around Pile Groups Using Neural Network and Adaptive Neuro-Fuzzy Inference System. *Applied Soft Computing* 9 (2):746–755. DOI: 10.1016/j.asoc.2008.09.006